SIMULTANEOUS FMRI AND METABOLIC IMAGING OF THE BRAIN USING SPICE

BY

RONG GUO

THESIS

Submitted in partial fulfillment of the requirements
for the degree of Master of Science in Electrical and Computer Engineering
in the Graduate College of the
University of Illinois at Urbana-Champaign, 2018

Urbana, Illinois

Adviser:

Professor Zhi-Pei Liang

Abstract

In this thesis, we propose a novel approach to achieve simultaneous acquisition of high resolution MRSI and fMRI in a fast scan. The proposed acquisition scheme adds an EVI-based sequence module into a subspace-based imaging technique called SPICE (SPectroscopic Imaging by exploiting spatiospectral CorrElation). With the features of ultrashort TE/short TR, no water and lipid suppression, extended k-space coverage by prolonged EPSI readout and highly sparse sampling, the data acquisition captures both the spatiospectral information of brain metabolites and the dynamic information of brain functional activation. The data processing and reconstruction are based on the subspace modeling and involve pre-trained basis functions and spatial prior information. Moreover, the complementary information between fMRI and MRSI is utilized to further improve the quality of both fMRI and metabolic imaging. The in vivo experimental results demonstrate that the proposed method can achieve whole brain covered, simultaneous fMRI at spatial resolution of 3.0 × 3.0 × 1.8 mm, temporal resolution 3 seconds, along with metabolic imaging at nominal spatial resolution of 1.9 × 2.3 × 3.0 mm in a single 6-minute scan. The high-quality metabolic maps, spatially resolved spectra, resting-state functional networks and task time courses corresponding to the task events can all be obtained in the in vivo scans. This technique, when fully developed, will become a powerful tool to study the brain metabolism and function activities.

Acknowledgments

My sincere appreciation first goes to my advisor Professor Zhi-Pei Liang, who supported and encouraged me throughout the process of this research and also my graduate education. His unwavering enthusiasm for science and technology kept me constantly engaged in my research and study.

My gratitude also extends to my colleagues Yudu Li and Yibo Zhao. Their talent, intelligence, and help have made this work possible. Thanks also go to Bryan Clifford, Tianyao Wang and Professor Yao Li for their support, experience, and thoughts about the field.

Finally, I would like to thank my family and my close friends, especially my girlfriend Yucheng, for their love, understanding and support.

Contents

1. Introduction

1.1 Motivation

Functional magnetic resonance imaging (fMRI) has been employed in a huge number of studies in cognitive neuroscience, clinical psychiatry, phycology, presurgical planning and therapy monitoring. It depicts the changes of blood oxygen level dependent (BOLD) signal modulated by brain activation and thus provides a powerful tool for noninvasively investigating the functional connection of the human brain. Magnetic resonance spectroscopic imaging (MRSI) is a complementary technique that provides the spatiospectral function of specific molecules. With the capability to map the distribution of biologically important molecules like NAA, creatine and glutamate, it promises to make a significant contribution in brain metabolism study, disease early detection, and characterization and evaluation of clinical therapeutic efficacy.

fMRI and MRSI provide rich complementary biological information about the brain metabolism, related to cognitive and chemical dynamic processes. Both techniques reflect the health status of the brain in different respects. Currently, fMRI and MRSI experiments are performed in two separate scans using different data acquisition schemes. More specifically, the most widely used fMRI protocols employ the gradient-echo based, multi-slice, echo planar imaging (EPI) sequence to collect a sequence of T2*-weighted images [1]–[6]. The spatial resolution is about 3 mm, temporal resolution is about 3 seconds and the entire scan usually lasts about 8-10 minutes. But such an acquisition scheme is vulnerable to the chemical shift effect, field inhomogeneity, field fluctuation and susceptibility effect [5]–[6]. To obtain the spatiospectral functions of different molecules, MRSI techniques need to acquire both spatial and spectral encoding, thus resulting in low spatiotemporal resolution [7]–[10]. Most of the current MRSI techniques are based on chemical shift imaging (CSI) or echo planar spectroscopic imaging (EPSI) trajectory which usually result in spatial resolution of centimeters and total scan time on the order of half an hour [8], [9], [11]–[13]. Furthermore, the low signal-to-noise ratio (SNR), large

overwhelming tissue water and lipid signals along with the poor spatial resolution and long acquisition time have made the MRSI applications very challenging and limited. Given these technical limitations, there have been few studies linking brain metabolism and functional activities using fMRI and MRSI. But the connection or combination of metabolic imaging and functional imaging has been the dream of MR scientists for a long time. The current attempts to combine fMRI and MRSI are largely limited in the studies using single voxel spectroscopy (SVS) and called functional MR spectroscopy (fMRS) [14]–[17]. In these studies, the investigations are limited in a single voxel with size of centimeters, which suffers from severe partial volume effect and limited brain coverage [14]–[23]. Moreover, the fMRI scans are performed separately with the fMRS scans, which can introduce bias in the observation of subject functional process during the fMRS scans.

Over the past decades, significant efforts have been made to overcome these difficulties. For example, the parallel imaging technique [24], [25] which utilizes the multi-coil encoding information, the simultaneous multi-slice technique which excites multi-slice in one TR [26], the more efficient sampling trajectory like echo-planer trajectory, spiral trajectory and concentric ring trajectory and various advanced reconstruction methods have been proposed [11], [27]. Especially, a subspace model proposed by Professor Zhi-Pei Liang [28], [29] broke the limitation of traditional Fourier imaging framework and makes fast, high resolution imaging possible. This subspace modeling has been developed into a fast imaging scheme by incorporation with fast data acquisition, constrained reconstruction, and physical and learning based spectral prior information, which is able to achieve ultra-fast MR spectroscopic imaging by the name of SPICE (SPectroscopic Imaging by exploiting spatiospectral CorrElations). With the SPICE technique, one can achieve high-resolution MRSI data at around $3\times3\times3$ mm^3 in a single 5 minute scan. Also, the unsuppressed water spatiospectral signals can provide various information, e.g. field drift, field inhomogeneity map, relaxation map (T2*), susceptibility distribution (QSM) [30] and so on.

This thesis work aims at extending the technical progress of SPICE and developing a new data acquisition and reconstruction scheme for high-resolution simultaneous mapping of brain metabolism and function through simultaneous fMRI and MRSI.

1.2 Main Results

In this work, we propose a new data acquisition and processing framework by extending the subspace-based imaging framework to simultaneously acquire high resolution fMRI and MRSI signals with high speed. The main results of this work are summarized as follows:

First, we propose a novel data acquisition scheme which enables the acquisition of both fMRI and MRSI in the same time scale. This acquisition can achieve MRSI of nominal spatial resolution at $2.0\times2.4\times3$ mm^3 and fMRI of spatial resolution at 3 mm^3 and 3 second temporal resolutions in a 6-minute scan, covering the whole brain with FOV as $230\times230\times72$ mm^3.

Second, with the proposed data acquisition scheme, we used the subspace modeling and optimization algorithms to effectively reconstruct the metabolite spatiospectral functions from the water-unsuppressed MRSI signals and the fMRI images from the highly sparse sampled EVI data.

Finally, the proposed approach has been evaluated using in vivo experimental data, which shows that the high quality, high resolution metabolic mapping as well as both the resting-state functional networks and the task based functional activities can be obtained successfully. This unprecedented imaging capability to simultaneously map brain metabolism and brain function will become a powerful tool in both scientific and clinical settings.

1.3 Organization of the Thesis

This thesis is organized as follows:

Chapter 2 reviews the literature related to the development of magnetic resonance spectroscopic imaging (MRSI), functional magnetic resonance imaging (fMRI) and functional magnetic resonance spectroscopy (fMRS) which are the primary tools in the MR field to study the brain metabolism and functional activities. Also, the basic mathematical

tools for subspace modeling we used in this work, known as partial separability (PS) model and low tensor model, are introduced. Then, the recently proposed fast high-resolution magnetic resonance spectroscopic imaging technique, known as SPICE, is presented.

Chapter 3 introduces the details of the data acquisition scheme used for simultaneous acquisition of both MRSI and fMRI signals, which include the pulse sequence design, timing arrangement, key parameter and features, k-space sampling and trajectories for both MRSI and fMRI signals collection. Moreover, the detailed experimental setup and protocols for both resting-state and task functional experiments are presented.

Chapter 4 describes the image reconstruction algorithms and processing methods. It includes the basic subspace signal model that most of the processing steps are based on, the detailed problem formulation and solutions for the signal reconstruction for both fMRI and MRSI datasets, and also a brief description of the potential of this technique to utilize the complementary information between fMRI and MRSI to enable improvement of reconstruction quality and removal of signal artifacts.

Chapter 5 shows the results can be obtained using the proposed approach. The high quality MRSI results including the reconstructed metabolite spatial distribution and spatially resolved spectra, as well as the fMRI results including resting-state functional networks and the time course with corresponding network structures, are all presented.

Chapter 6 concludes this thesis.

2. Background

2.1 MRSI, fMRI and fMRS

MRSI is the technique to acquire the spatiospectral functions of the imaging objects. Different from the traditional magnetic resonance imaging (MRI) which aims at acquiring spatial distribution, MRSI needs to encode both spatial and spectral information. The extra dimension leads to longer scan time and lower resolution. The MRSI signals can be modelled as:

$$s(\boldsymbol{k_n}, t_m) = \int_V \int_W \rho(\boldsymbol{r}, f) e^{-i2\pi f \cdot t_m} e^{-i2\pi \boldsymbol{k_n} \cdot \boldsymbol{r}} e^{-i2\pi \nabla f(\boldsymbol{r}) \cdot t_m} df d\boldsymbol{r} + \xi \qquad (2.1)$$

Most of the interest in the ^{1}H-MRSI community focuses on investigating the spatiospectral functions of specific molecules in the brain like N-acetyl-aspartate (NAA), creatine (Cr), choline (Cho), glutamine (Glu) and so on. The concentrations of these molecules are usually several orders of magnitude lower than that of tissue water and lipid, so the signal-to-noise ratio (SNR) is low in traditional scans. The low SNR, low resolution, long scan time and large nuisance signals from tissue water and lipid have greatly limited the development and application of MRSI technique. Great efforts have been made by the research community to push this field forward. For example, the following approaches have been proposed to overcome those difficulties: fast scanning techniques like echo-planar spectroscopic imaging (EPSI) [11] and spiral spectroscopic imaging [27]; sparse sampling methods including SLIM (spectral localization by imaging) [31], parallel imaging using information from multi-coil encoding [24], [25], compressed sensing [32], low rank modeling [33] and super-resolution [34]; and advanced excitation and localization methods like PRESS, STREM, LASER and semi-LASER [35]–[38]. However, the resolution of the state-of-the-art methods is still around a centimeter and the scan time is about half an hour.

fMRI is another complementary imaging technique used to study the brain function non-invasively. It has been employed in a huge number of studies in cognitive neuroscience, clinical psychiatry, phycology, presurgical planning and therapy monitoring. It depicts the changes of blood oxygen level dependent (BOLD) signal modulated by brain activation and thus provides a powerful tool for investigating the functional connection of the human brain. Current fMRI techniques are mostly based on the multi-slice EPI technique, which can collect one image of the brain in 1-3 seconds. But the EPI sequence suffers from chemical shift, geometric distortion, and signal loss. In the past 30 years, many techniques have been developed to increase the spatiotemporal resolution, remove the artifacts and analyze brain functions. These include fast imaging acquisition such as simultaneous multi-slice acquisition and spiral trajectory, reconstruction approaches such as parallel imaging, compressed sensing, and low-rank modeling [24], [25], [32], and analysis methods such as the seed-based method, ICA-based method and graph-based method [39]–[41]. Taking the ICA method as an example, the fMRI image series can be expressed as:

$$s(\boldsymbol{x}, T) = \sum_{i=1}^{I} W_i(\boldsymbol{x}) X_i(T) \tag{2.2}$$

where I is the total number of independent components, the temporal components $\{X_i(T)\}$ are statistically independent with each other and the $\{W_i(x)\}$ are the spatial coefficients of each independent component and thus can represent the functional networks.

Functional MR spectroscopy (fMRS) is the technique currently used for studying the neurochemical changes in response to the brain functions. It repeats acquisition of single voxel spectroscopy (SVS) of the human brain when the subjects are instructed to perform specific tasks or receive stimulation. Thus, it can detect the dynamic changes of metabolites or neurochemicals when the brain goes through functional changes. Many studies of metabolism and brain function coupling using fMRS have achieved exciting results [14]–[19], [21]–[23], [42]–[45]. However, the current fMRS technique is limited by its low spatial resolution (around 2 centimeters), small brain coverage (only single voxel measurements) and low SNR. Therefore, the studies usually involve a group of subjects to achieve enough statistical power. Also, to localize the functional region and detect brain

functional process, fMRI scans are performed separately, which may cause bias between the detected functional process by fMRI and the actual one during fMRS.

2.2 Partial Separability and Subspace Model

In this section, we review the theoretical foundation for the subspace-based imaging framework, specifically, the partial separable function (PSF). Partial separability, proposed by Professor Zhi-Pei Liang in 2007, leads to the development of the subspace-based imaging technique and its applications in dynamic imaging and spectroscopic imaging [29].

Consider a multivariate image function $f(x_1, x_2, \ldots, x_d)$, which is common in current MR imaging techniques like dynamic imaging and spectroscopic imaging. The dimensions can include 3 spatial dimensions, 1 or 2 temporal dimensions, 1 or 2 spectral dimensions, multi-channel and even multi-contrast, depending on the applications. Under these problem settings, the encoding number needed for imaging increases exponentially when the dimension increases, which will lead to extremely long scan time and low resolution. To overcome the difficulties, how to represent the image functions in a most efficient way and how many true degrees of freedom are needed to represent the signals become critical issues. The partial separability model is one of the most influential models. It represents the multi-dimensional functions as:

$$f(x_1, x_2, \ldots, x_d) = \sum_{l=1}^{L} \phi_{l,1}(x_1)\phi_{l,2}(x_2)\cdots\phi_{l,1}(x_1) \tag{2.3}$$

which is called *L*-th separable. The model always holds when the order L goes to infinity. In the imaging problem, the order L is usually smaller than the $x_1 \times x_2 \times \cdots \times x_d$, which means that the underlying degrees of freedom to represent the imaging functions are fewer and the encoding number needed can be reduced. Usually, the $x_1, x_2, \ldots, x_d$ can represent the variables for different physical meaning. For example, in spectroscopic imaging, x_1 can represent the spatial location (including 3 dimensions x, y and z) and x_2 can represent

the specific frequency. In this case, we usually present the spatiospectral function in $(\boldsymbol{k}, t)$ space. Then, the partial separability of the signal can be expressed as:

$$s(\boldsymbol{k}, t) = \sum_{l=1}^{L} c_l(\boldsymbol{k})\varphi_l(t) \tag{2.4}$$

which is true if and only if the following conditions hold:

Assume that $s(\boldsymbol{k}, t)$ is defined over space $\mathcal{K} \times \mathcal{T}$ and $\mathcal{K} = \{k_1, k_2, \dots, k_n\}$ and $\mathcal{T} = \{t_1, t_2, \dots, t_n\}$, denote:

$$\mathbf{C} = \begin{bmatrix} s(\boldsymbol{k_1}, t_1) & s(\boldsymbol{k_1}, t_2) & \cdots & s(\boldsymbol{k_1}, t_m) \\ s(\boldsymbol{k_2}, t_1) & s(\boldsymbol{k_2}, t_2) & \cdots & s(\boldsymbol{k_2}, t_m) \\ \vdots & \ddots & & \vdots \\ s(\boldsymbol{k_n}, t_1) & s(\boldsymbol{k_n}, t_2) & \cdots & s(\boldsymbol{k_n}, t_m) \end{bmatrix} \tag{2.5}$$

If and only if $\mathbf{C}$ is rank L and $L < \min\{m, n\}$, then equation (2.4) holds.

This model implies that if the imaging function is partial separable with a small order L, then the parameters we need to represent the spatiospectral functions will significantly reduce, which enables a subspace-based fast imaging scheme for MRSI, which is known as SPICE [28], [46].

2.3 SPICE

The SPICE framework includes several key features to enable rapid, high resolution spectroscopic imaging: 1) Extended (k,t) space coverage using sparse sampling to achieve high spatial resolution; 2) Pre-determined spectral basis functions; 3) Constrained reconstruction on sparsely sampled data by involving bases functions and spatial prior information.

As shown in Fig. 2.1, the imaging data are acquired with fast EPSI sequence to achieve large k-space coverage but temporally under-sampled. The training data to derive basis functions can be obtained with various acquisition schemes. The example shown in Fig. 2.1 is a CSI sequence which acquires MRSI signals in high temporal resolution but low

spatial resolution. The estimation of the basis functions can be done by SVD based method [28] or machine learning. The reconstruction from the sparse data is done by estimating spatial coefficients in the subspace modeling:

$$\widehat{\boldsymbol{C}} = \arg\min_{\boldsymbol{C}} \left|\left|\boldsymbol{d} - \Omega\mathcal{F}_B(\boldsymbol{C}\boldsymbol{\Phi})\right|\right|_2^2 + \lambda R(\boldsymbol{C}) \tag{2.6}$$

where $\boldsymbol{d}, \boldsymbol{C}, \boldsymbol{\Phi}$ are matrix representations of measured sparse data, spatial coefficients to be estimated and pre-determined bases functions, respectively. The R is a regularization function to impose any valid prior information. Then the metabolite spatiotemporal functions can be composed as equation (2.4).

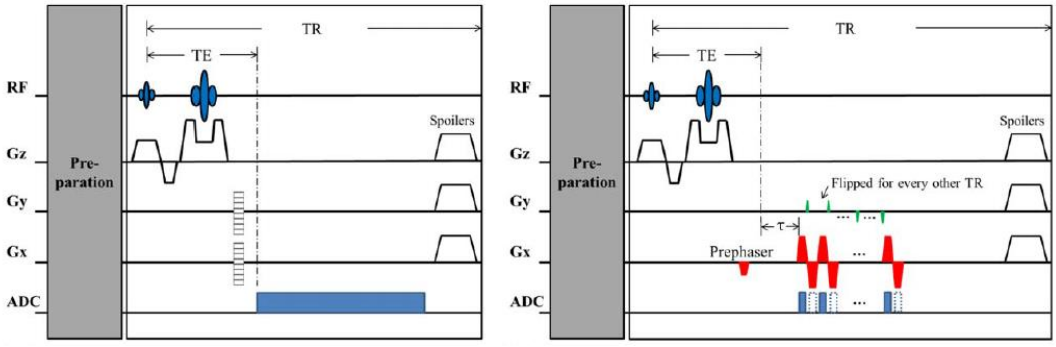

Figure 2.1: An example of the acquisition scheme for SPICE. Left figure: a CSI sequence to acquire the MRSI signal with high temporal resolution but low spatial resolution, which is used for estimating the spectral bases functions. Right figure: an EPSI sequence to achieve the MRSI signals with large k-space coverage but sparse sampling in the temporal direction.

3. Data Acquisition

In this chapter, we present the proposed data acquisition scheme to enable the simultaneous acquisition of fMRI and MRSI signals of the human brain in high resolution. The details about fMRI-MRSI interleaving, sparse sampling for fMRI and MRSI, and the implementation for in vivo studies are included.

3.1 Interleaved Scheme for fMRI and MRSI Acquisition

In the proposed data acquisition scheme, the fMRI and MRSI signals are acquired in an interleaving fashion (as shown in Fig. 3.1). Interleaving means that the fMRI and MRSI signals are collected in different TRs. We first collect N_1 TRs for MRSI, then N_2 TRs for fMRI, then N_1 TRs for MRSI and so on. This cycle repeats until the end of the scan. With this hybrid fMRI/MRSI acquisition strategy, the fMRI and MRSI signals are acquired in the same time scale, which achieves simultaneity. The key points for designing this hybrid fMRI/MRSI scheme include: 1) No water suppression for both fMRI and MRSI; 2) length of TR; 3) choice of N_1 and N_2; 4) choice of sequence type for collecting fMRI and MRSI signals.

1) As we know, the intensity of metabolite signals like NAA, creatine are several orders of magnitude lower than that of water due to the low concentrations of these molecules. So, in typical MRSI experiments, water suppression is usually required. However, the fMRI signals originate from the BOLD effect, which is the changes of water signals due to functional modulation. Suppression of the water signals in MRSI will also suppress the fMRI signals. Therefore, in this sequence, no water suppression is employed, which makes it possible to acquire the fMRI and MRSI signals simultaneously. Instead of using a long spectral selective pulse chain to suppress water signals physically [47], the removal of water signals is done using a signal processing tool [48]. The elimination of water suppression also enables us to achieve a very short TR for both fMRI and MRSI.

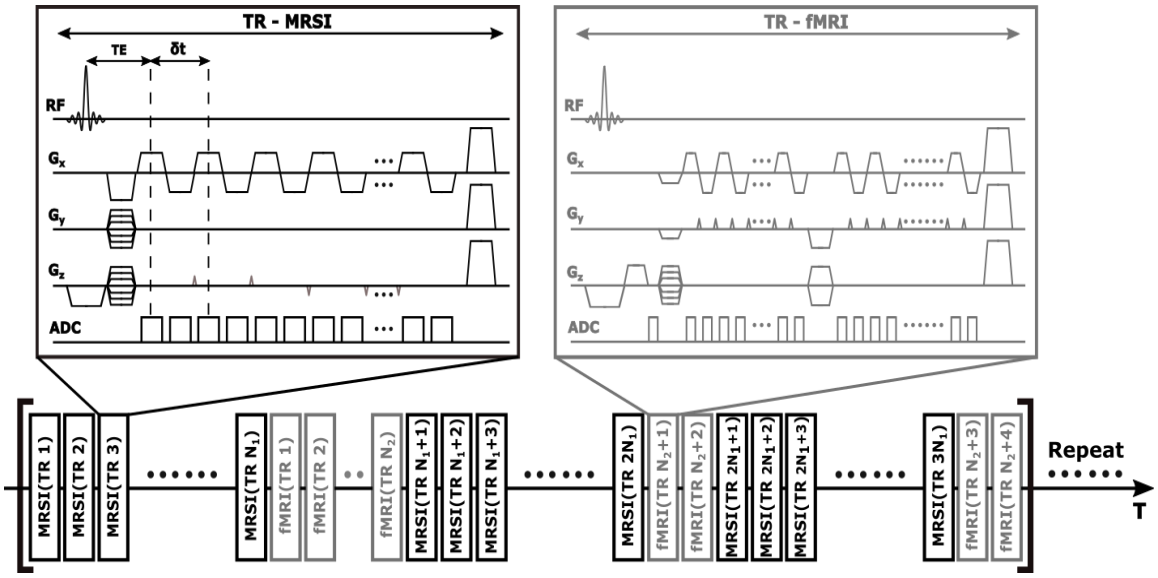

Figure 3.1: The proposed data acquisition scheme for collecting fMRI and MRSI signals in an interleaving fashion. A set of N_1 TRs is for sampling MRSI signals and then a set of N_2 TRs for fMRI signals. The cycle of fMRI and MRSI is repeated until the end of the scan. The sequence for MRSI acquisition is based on EPSI trajectory and the sequence for fMRI is based on EVI trajectory.

2) The choice of TR is not a trivial issue. For MRSI, different TRs have different SNR efficiency. As mentioned above, the SNR of metabolite signals is usually very low, so the choice of TR must take the SNR efficiency into account. The calculated result of SNR efficiency of an FID-based MRSI sequence is shown in Fig. 3.2. The TR larger than 100 ms can guarantee a good SNR efficiency and the peak point appears at around 300 ms. For fMRI, the TR values in the typical EPI-based sequence are usually less than 100 ms. It should be noted that the TR here is mentioned as time between two neighboring excitations but not neighboring excitations on the same volume as is its typical definition. The advantages of short TR include higher temporal resolution and weaker geometric distortion and susceptibility effect. However, in this interleaved sampling scheme, the values of TR for MRSI and fMRI need to be the same. Otherwise, it will destroy the steady state built for both fMRI and MRSI. Designing the sequence requires finding a good tradeoff.

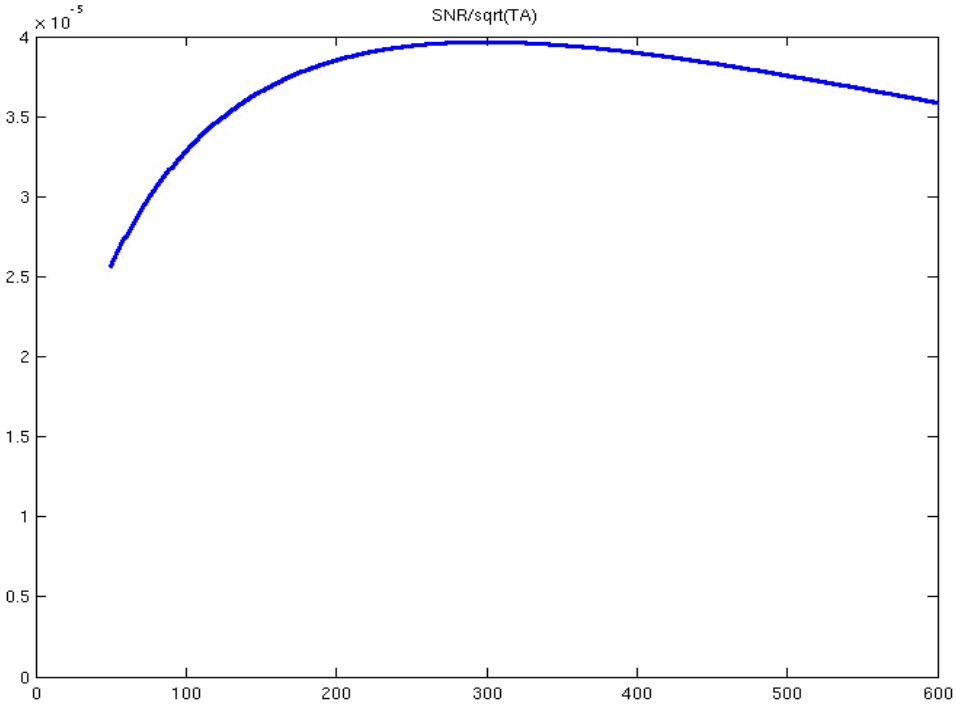

Figure 3.2: The SNR efficiency curve (for NAA signal) calculated based on the setting of FID-based MRSI sequence: T1 = 1400 ms, T2 = 240 ms, TE = 4 ms, BW = 167 kHz, dt = 1.76 ms, FA = Ernst angle.

3) The choice of N_1 and N_2 mainly depends on the temporal resolution desired for fMRI. The temporal resolution of fMRI depends on two major factors: frequency of BOLD signals and enough frames for statistical power. As we know, the frequency of BOLD signals is around 0.01~0.1Hz, so according to the Nyquist principle, the smallest temporal resolution of fMRI should be 5 seconds. In a typical fMRI sequence, the temporal resolution is around 3 seconds. Moreover, to have enough statistical power to separate the BOLD signals from physiological signals and also draw conclusions, typical fMRI experiments last for around 8 minutes and result in more than 150 frames. So the requirement of N_1 and N_2 should be:

$$(N_1 + N_2) \times TR \leq 3\ sec$$

4) The sequences used for MRSI and fMRI are discussed in the following sections. Basically, they should both be volume excitation so that the steady state can be kept. And

from the consideration of scanning speed and efficiency, the sampling of MRSI is based on EPSI trajectory and the sampling of fMRI is based on EVI trajectory.

3.2 SPICE-Based Sequence for MRSI Acquisition

As shown in Fig. 3.1, the sequence for acquisition of the MRSI signals is based on the SPICE sequence [28], [46] which uses an EPSI trajectory. However, the sequence is distinguished from the typical EPSI sequence for MRSI in the following aspects:

1) No water and the lipid suppression. As mentioned in section 3.1, the MRSI acquisition eliminates the suppression pulses, which enables the simultaneous acquisition of both MRSI and fMRI. Maintaining the water signals also provides lots of advantages. For example, the water signal can work as a reference for metabolite signals to perform absolute spectral quantification. Moreover, the spatiospectral functions of water and lipid signals can provide the high-resolution field map and lipid distribution to help fMRI signals to overcome chemical shift effect and geometric distortion due to the field variation. There are also potentials in extracting more information in water signals without any additional acquisition effort [30].

2) EPSI readout on FID signals. EPSI readout simultaneously encodes both spatial and spectral dimension, thus it can achieve a higher efficiency and speed than traditional CSI based readout, which only encodes the spectral dimension for each TR. One potential problem with EPSI readout is the inconsistency between odd and even echoes due to the eddy current. One alternative is using fly-back EPSI which uses only half of the EPSI data. The strategy used in our design is to utilize both odd and even echoes and correct the inconsistency in post-processing steps. The readout is sampled on free induction decay (FID) signals instead of the typical spin echo signals. FID-type acquisition is usually more sensitive to field inhomogeneity than spin echo because its decay follows T2* decay instead of T2 decay for spin echo. However, it can achieve much shorter TE and TR, which is important for reducing the acquisition time.

3) Ultra-shorter TE and short TR. The TE of the acquisition scheme can be pushed to lower than 4 ms. Short TE has several advantages. First, short TE can preserve the SNR because

the shorter the TE, the less decay. Second, short TE can preserve some signal components like macromolecule. As we know, some molecules have short T2 which means it will decay out and the sequence with long TE will not have the capability to detect. The direct benefit of short TR is shorter scan time. However, the short TR limits the spectral resolution which will affect the capability to separate different spectral peaks. In our scheme, this is overcome by subspace modeling, which is described in next chapter.

4) Extended readout with larger echo space. The comparison between the extended readout and standard EPSI is displayed in Fig. 3.3. The length of typical EPSI is usually limited to keep a small echo space (time interval between neighboring echoes) for satisfying Nyquist rate of metabolite signals. The proposed prolonged readout can result in a larger k-space coverage (kx direction) but with larger echo space which may violate the Nyquist rate. This sparse sampling in the spectral direction is also overcome by the subspace modeling. The resolution improvement brought by the extended readout can lead to better water and lipid removal results.

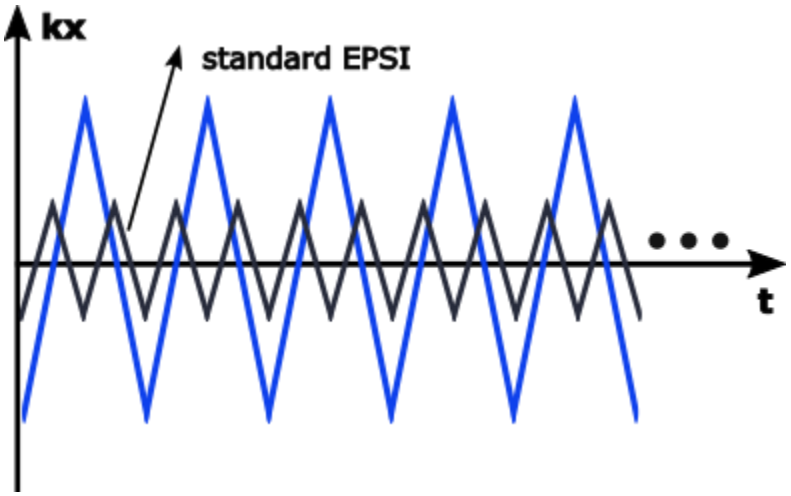

Figure 3.3: Comparison of extended EPSI readout and standard EPSI readout. The proposed EPSI readout has larger k-space coverage but larger echo space.

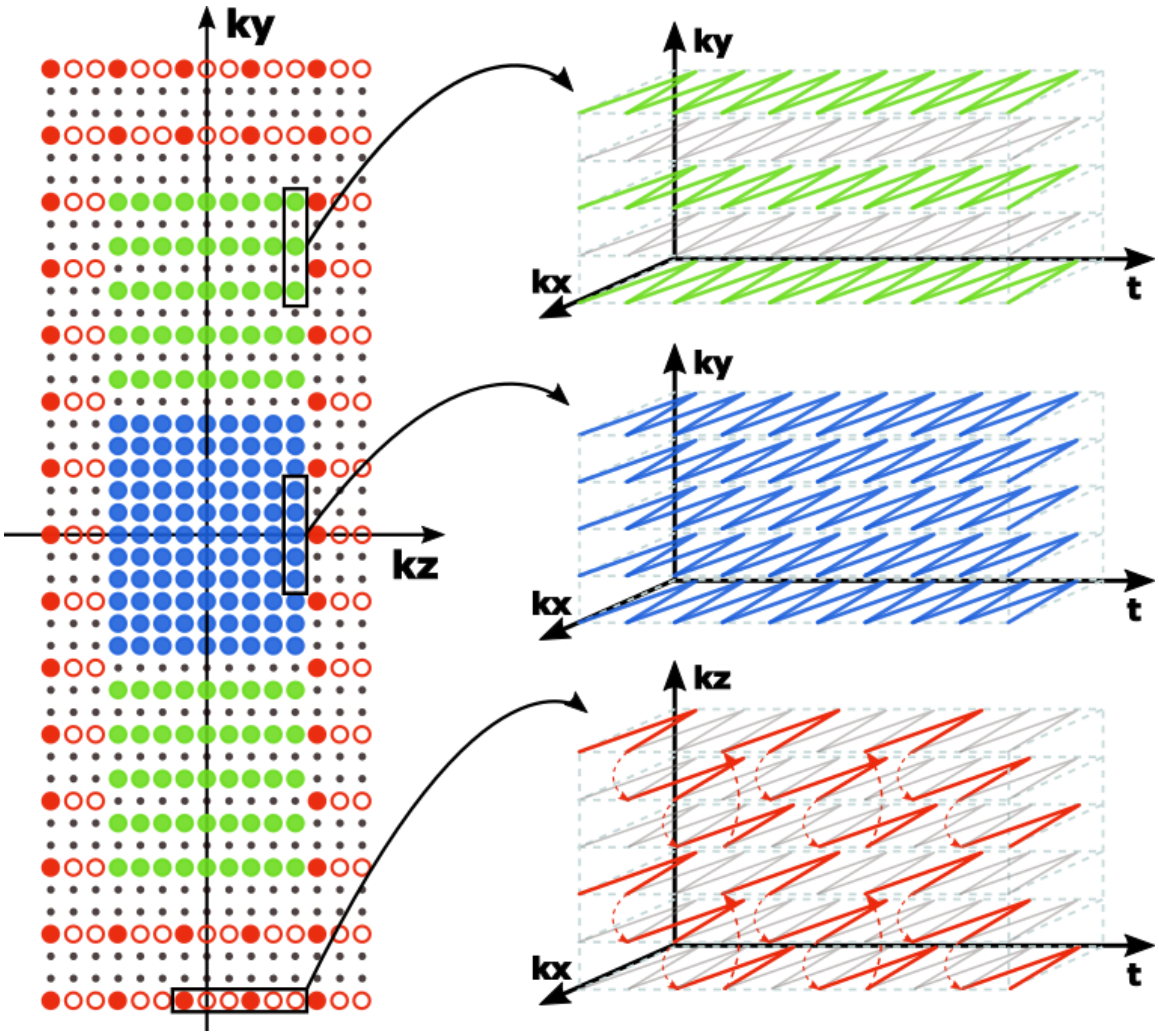

Figure 3.4: The sampling pattern in phase encoding for MRSI acquisition and its corresponding temporal sampling. The central region (blue) is fully sampled in both spatial and temporal direction. The outer region (green) is spatially under-sampled but the outside region (red) is sparsely sampled both spatially and temporally using blip gradient.

5) Sparse sampling in phase encoding. To further extend the k-space coverage and achieve higher resolution, the sparse sampling is employed in phase encoding directions (ky and kz). As shown in Fig. 3.4, a variable density is used in sparse sampling. The whole ky-kz space is divided by 3 regions. The central region where most of the energy resides is fully sampled both spatially and temporally to preserve enough SNR. Then, the neighbor region in ky is under-sampled by a factor of 2. The missing data in this region can be interpolated using parallel imaging technique [24], [25] where the interpolation kernel can be estimated

from the k-space center. The outer k-space is sparsely sampled both spatially and temporally using blipped gradient (Fig. 3.4). This acquisition strategy can effectively extend the k-space coverage. The aliasing caused by under-sampling in both spatial and spectral direction can be fixed by parallel imaging and subspace modeling.

In summary, the proposed sequence for MRSI acquisition keeps the basic features of SPICE sequences which include 1) no water and lipid suppression; 2) EPSI readout on FID-signals; 3) ultra-short TE and short TR; 4) extended EPSI readout with larger echo space; 5) extended k-space sampling using variable density.

3.3 EVI-Based Trajectory for fMRI Acquisition

As shown in Fig. 3.1, an EVI-based trajectory is used for fMRI signals acquisition. There are also several key features in designing the sequence: 1) embedded field drift navigator; 2) multi-shot EVI encoding; 3) sparsely sampling in both spatial and temporal directions.

1) Embedded field drift navigator: during each TR of the fMRI data acquisition, we first turn on the ADC to collect an FID signal for a very short period (around 1 ms) immediately after the pulse excitation. This FID signal will be used for tracking B0 field drift and this information can be used to correct the inconsistency in both MRSI and fMRI data caused by field drift.

2) Multi-shot EVI encodings: after collection of the field drift navigator, we turn on echo-planar encoding gradients to collect imaging data in echo-volume-imaging trajectories (see Fig. 3.5). To compose a complete k-space for fMRI images, the encodings from multiple TRs are combined. For example, in the current implementation, within a single TR, 5 slices of k-space are collected so 8 TRs are needed to form a complete 40 slices of the k-space. To minimize the inconsistency and achieve a good point spread function, all 8 TRs start the sampling from central k-space and then proceed to outside slices of k-space. Due to the signal relaxation decay, this strategy can preserve the good SNR in central k-space slices and remove the effect of noise and field inhomogeneity in outside k-space slices. Note that in implementing our EVI sampling trajectories, ramp sampling is used along the readout direction (kx) to further increase the spatial resolution.

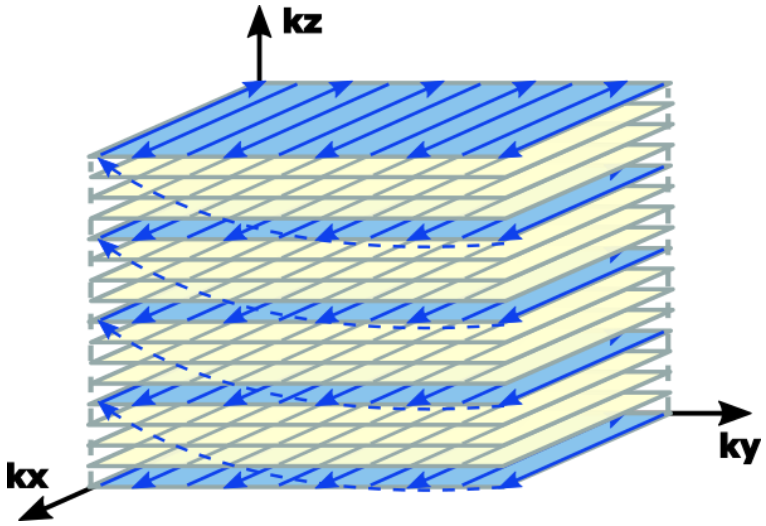

Figure 3.5: The k-space trajectory of multi-shot EVI sequence. 5 slices of k-space are sampled in each TR. The sampling from one slice to another slice is done using blipped gradient.

3) Sparse sampling in both spatial and temporal directions. To utilize the multi-channel acquisition and obtain enough spatial resolution, we collect 76 frequency-encodings along kx, 38 phase encodings along ky, and 5 phase encodings in kz in each TR. Thus, in one fMRI frame, 8 TRs can compose a complete fMRI data frame with 76×76×40 k-space coverage (a factor of 2 under-sampling along both ky). To improve temporal resolution and also take advantage of the partial separability [29] of fMRI signals, temporal under-sampling is applied. More specifically, we collect one "full" 8-TR fMRI data frame every 3 frames which takes about 9 seconds. In between two 8-TR fMRI frames, we collect two under-sampled 2-TR fMRI data frames (it is equivalent to a factor of 4 under-sampling along kz). So, the effective temporal resolution of the fMRI data can reach 3 seconds as shown in Fig. 3.6.

In summary, the fMRI acquisition is based on multi-shot EVI sampling trajectory. Involving both multi-coil acquisition and subspace modeling, it can achieve both high spatial resolution and high temporal resolution.

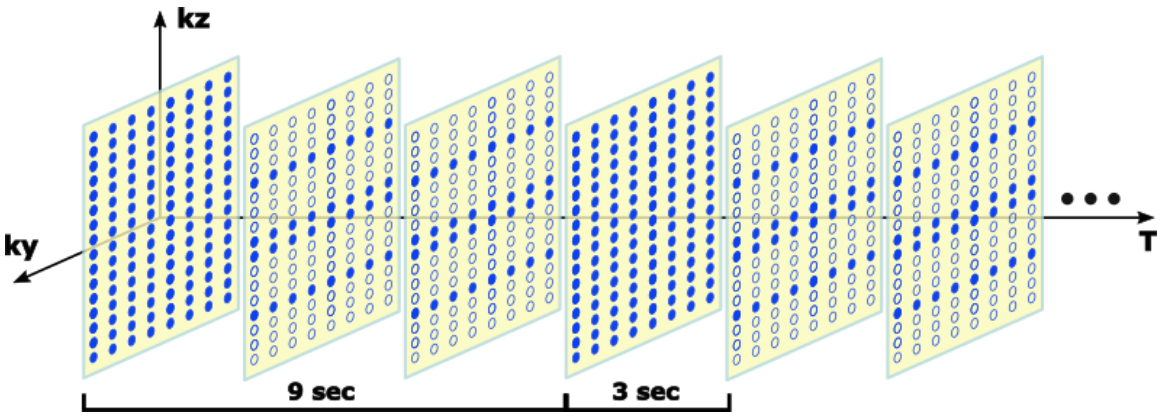

Figure 3.6: The (k,T) sampling of fMRI signals. The "full" 8-TR fMRI frames are acquired every 9 seconds. In between two 8-TR fMRI frames, two 2-TR fMRI data frames (with a factor of 4 under-sampling along kz) are collected. This scheme results in 3 seconds effective temporal resolution of the fMRI images.

3.4 Implementation for Experimental Studies

Proton MRSI experiments with the proposed data acquisition scheme were conducted on healthy volunteers on a 3T scanner (Siemens Prisma) with a 20-channel head array coil. Our implementation of the sequence used a 27° excitation, TR = 160 ms, TE = 1.6 ms, readout bandwidth = 167 kHz, and field of view (FOV) = 230 × 230 × 72 mm with two outer volume suppression (OVS) bands over the top and bottom slices to eliminate aliased signals from outside the excitation volume. The MRSI encoding has 120 × 96 × 24 k-space points, which results in the resolution of 1.9 × 2.3 × 3.0 mm while the fMRI encoding has 76 × 76 × 40 k-space points to achieve a 3.0 × 3.0 × 1.8 mm resolution. The echo-space of MRSI encoding is 1760 μs and the frame rate of fMRI series is 3 seconds. The whole scan for this sequence took 6 minutes with dummy pulses to approach steady state and calibration scans for bipolar correction.

To validate the capability of the proposed scheme to detect functional activation, both resting-state and task-based functional experiments are performed. In the resting-state section, the subjects are instructed to rest with eyes open and fixate on a cross-hair. In the motor task section, the subjects are instructed to perform finger tapping with the right hand.

In the visual task section, the periodic visual stimulation was projected on screen in the task period while a cross-hair was displayed in the rest period. In both motor and visual task scans, the rest-task cycle is 40s – 20s from start to the end of the sequence.

The experimental protocol also included a T1-weight anatomical scan using MPRAGE sequence at 1 mm isotropic resolution (TR/TE/TI = 1900/2.29/900 ms, flip angle 9°). To provide a reference point of the functional network, a conventional BOLD EPI sequence was also run covering the same brain region (TR/TE = 2.5 s/30 ms, flip angle = 80°, Matrix size = 96 × 96 × 36, 160 frames were acquired in 6.8 minutes scan).

4. Image Reconstruction

In this chapter, we introduce signal processing algorithms to facilitate the high-quality reconstructions of both fMRI and MRSI signals. These reconstructions and processing are based on subspace modeling, which has been widely used in dynamic imaging and spectroscopic imaging. This chapter will also include the advantages of using the complementary information from both fMRI and MRSI to improve each other's image quality and stability.

4.1 Signal Model

Given the data acquisition scheme as described in chapter 3, it will generate two data sets simultaneously, $d_1(\boldsymbol{k}, T)$ and $d_2(\boldsymbol{k}, t)$, from which fMRI images and metabolic spatiospectral functions are reconstructed, respectively. Note that different variables related to time, t and T, are used to represent signal changes at different time scales. More specifically, for the fMRI data set, $\mathrm{d}_1(\mathbf{k}, \mathrm{T})$, $T = n_1 \mathrm{TR}$, which means the time along the TRs, while for the MRSI data set, $\mathrm{d}_2(\mathbf{k}, \mathrm{t})$, $\mathrm{t} = \mathrm{n}\delta\mathrm{t}$, with $\delta\mathrm{t} = 1.76$ ms, which means the time along echo space in one TR. In other words, the MRSI data are collected with high temporal resolution around milliseconds to provide enough spectral bandwidth to cover the spectral distributions of different molecules and the collection along the TRs are summed together to form a complete 4D MRSI dataset. The fMRI data are acquired at lower temporal resolution of seconds to capture BOLD signal changes. These two datasets can be expressed as:

$$d_1(\boldsymbol{k}, T) = \int_0^{t_f} \left(\Omega_1(\boldsymbol{k}, t, T) \mathcal{F}_{\boldsymbol{x}-\boldsymbol{k}} \left(\mathcal{F}_{f-t} \left(\rho(\boldsymbol{x}, f, T) \right) \right) + \eta(\boldsymbol{k}, t, T) \right) dt \tag{4.1}$$

$$d_2(\boldsymbol{k}, t) = \int_0^{T_A} \left(\Omega_2(\boldsymbol{k}, t, T) \mathcal{F}_{\boldsymbol{x}-\boldsymbol{k}} \left(\mathcal{F}_{f-t} \left(\rho(\boldsymbol{x}, f, T) \right) \right) + \eta(\boldsymbol{k}, t, T) \right) dT \tag{4.2}$$

where $\rho(\boldsymbol{x}, f, T)$ denotes the spatio-spectral distribution of the signals of all the molecular components including water, lipids, metabolites, etc., along the scan period. $\eta(\boldsymbol{k}, t, T)$ is

the measurement noise which is assumed to be complex white Gaussian noise. $\mathcal{F}_{f-t}$ and $\mathcal{F}_{\boldsymbol{x}-\boldsymbol{k}}$ are 1-D and 3-D Fourier transform along frequency-time direction and k-space-image directions, respectively. $\Omega_1(\boldsymbol{k}, t, T)$ and $\Omega_2(\boldsymbol{k}, t, T)$ are the sampling operator in k-space for fMRI and MRSI measurement as described in data acquisition. Since the sampling of both data sets in (k, T)-space and (k, t)-space is sparse, we need special algorithms for data processing and image reconstruction.

4.2 Reconstruction of MRSI Spatiotemporal Functions

MRSI data processing is based on a union-of-subspaces model, with which we can express the overall spatiospectral function as:

$$\rho_{MRSI}(\boldsymbol{x}, t) = \rho_w(\boldsymbol{x}, t) + \rho_f(\boldsymbol{x}, t) + \rho_{MM}(\boldsymbol{x}, t) + \rho_m(\boldsymbol{x}, t)$$
$$= \sum_{l_w}^{L_w} U_{l_w}(\boldsymbol{x}) V_{l_w}(t) + \sum_{l_f}^{L_f} U_{l_f}(\boldsymbol{x}) V_{l_f}(t) + \sum_{l_{MM}}^{L_{MM}} U_{l_{MM}}(\boldsymbol{x}) V_{l_{MM}}(t) + \sum_{l_m}^{L_m} U_{l_m}(\boldsymbol{x}) V_{l_m}(t) \quad (4.3)$$

where the $\rho_w(\boldsymbol{x}, t)$, $\rho_f(\boldsymbol{x}, t)$, $\rho_{MM}(\boldsymbol{x}, t)$, $\rho_m(\boldsymbol{x}, t)$ represent the spatiotemporal functions of water, lipid, macromolecules and metabolites, respectively. This low rank, subspace model assumes that each signal component should reside in a low-dimensional subspace spanned by a finite number of basis functions, i.e. $\{V_{l_w}\}$, $\{V_{l_f}\}$, $\{V_{l_{MM}}\}$ and $\{V_{l_m}\}$ with corresponding spatial coefficients $\{U_{l_w}\}$, $\{U_{l_f}\}$, $\{U_{l_{MM}}\}$ and $\{U_{l_m}\}$. This comes from the physical modeling that each signal component come from specific molecules and the total number of types of molecules and tissue types of the human brain should be limited and small.

To reconstruct the MRSI spatiospectral functions $\rho_{MRSI}(\boldsymbol{x}, t)$ from the sparsely sampled data $d_2(\boldsymbol{k}, T)$, the processing pipeline is based on the SPICE imaging framework and includes several key steps: a) correction of field drift using the field drift estimated from navigator signals, b) interpolation of spatially under-sampled data using parallel imaging, c) estimation and correction of field inhomogeneity using the unsuppressed water signals, d) removal of the water and lipid signals, and e) reconstruction of the spatiospectral functions from the temporally sparsely sampled data.

a) Correction of field drift. The field drift is inevitable in MR scanning especially in the cases when the gradient is pushed hard and switches quickly. The energy released by RF pulse and gradient switching can increase the temperature of the scanning environment, which causes the frequency drift of the main field B_0. As described in chapter 3, a short field drift navigator is collected in each TR of fMRI signals $d_1(\boldsymbol{k}, T)$. This short FID can be used for estimating field changes over time. We model the field drift changes along time as a 4-order polynomial function:

$$S(t,T) = S_0(T)e^{i2\pi\delta f(T)t}$$
$$\text{where:} \quad \delta f(T) = \sum_{i=0}^{4} a_i T^i \tag{4.4}$$

Therefore, we can calculate $\delta f(T)$ easily from the navigators and then apply it back to correct the field drift in MRSI data $d_2(\boldsymbol{k}, t)$.

b) Interpolation of spatially under-sampled data using parallel imaging. The theory behind parallel imaging is Papoulis' multi-channel sampling theorem [49]. It states that under some assumptions and conditions, the under-sampled bandlimited data can be recovered from multi-channel acquired data. The most widely used methods for parallel imaging are SENSE and GRAPPA [24], [25]. In this problem, the recovery of sparsely sampled k-space is done using a hybrid GRAPPA/SENSE method. We first reconstruct the first time point of $\mathrm{d}_2(\mathbf{k}, \mathrm{t})$ using GRAPPA. The interpolation kernel is estimated from the fully sampled central k-space data of the first several time points. Then the coil sensitivity maps are estimated from the GRAPPA reconstruction images in a sum of squares sense. With the estimated sensitivity maps, which are assumed to be echo independent, it is applied to reconstruct the remaining time points of $\mathrm{d}_2(\mathbf{k}, \mathrm{t})$ using the SENSE algorithm.

c) Estimation and correction of field inhomogeneity. Due to the elimination of water signals, the carried field inhomogeneity can be estimated from the unsuppressed water signals. As the model for FID signals:

$$S(x,t) = S_0(x)e^{\frac{-t}{T_2(x)}}e^{i2\pi f(x)t}e^{i2\pi df(x)t} \tag{4.5}$$

where the $df(x)$ represents the field map. Therefore, the estimation of $df(x)$ can be modelled as a linear prediction problem which can be efficiently solved with a HSVD algorithm [50]. After the high-resolution field map is obtained, it can be used to remove the field inhomogeneity term $e^{i2\pi df(x)t}$ in the MRSI signals, which is important for reducing the rank of the subspaces.

d) Removal of tissue water and lipid signals. The removal of water and lipid signals is done with a model-based approach proposed in [48], and the removal of water sideband is based on a reference-based method proposed in [51]. Details can be found in the reference and will not be discussed in this thesis.

e) Reconstruction of the spatiospectral functions from the temporally sparsely sampled data. $\rho_{\mathrm{MRSI}}(\mathbf{x}, \mathrm{t})$ is reconstructed from the pre-processed, noisy, water-lipid removed MRSI data based on subspace modeling as in the SPICE imaging framework. The reconstruction can be divided into two steps: estimation of spectral basis and estimation of spatial coefficients. The estimation of spectral basis functions is done using quantum simulated spectral basis and training data [28], [46]. The estimation of the spatial coefficients is done using a constrained optimization formulation:

$$\widehat{\boldsymbol{U}}_m = \arg\min_{\boldsymbol{U_m}} \left|\left|\boldsymbol{d}_1 - \Omega_1 \mathcal{F}_{x-k}(\boldsymbol{U_m V_m})\right|\right|_2^2 + \lambda \boldsymbol{R}(\boldsymbol{U_m}) \tag{4.6}$$

where $\boldsymbol{U_m}, \boldsymbol{V_m}$ are the matrix representation of spatial coefficients and estimated basis functions. λ is the regularization parameter and $\boldsymbol{R}$ is the chosen regularization function. After getting the spatial coefficients, the metabolite spatiotemporal functions can be reconstruction as:

$$\rho_m(\boldsymbol{x}, t) = \sum_{l_m}^{L_m} U_{l_m}(\boldsymbol{x}) V_{l_m}(t) \tag{4.7}$$

In summary, the reconstruction of MRSI signals is based on the subspace modeling and enables high quality reconstruction of metabolite signals from the non-water-suppressed data.

4.3 Reconstruction of fMRI Images

The processing of fMRI signals is also based on the subspace modeling. More specifically, we take advantage of the PS property of the fMRI signals $d_1(\boldsymbol{k}, T)$, which can be expressed as:

$$d_1(\boldsymbol{k}, T) = \sum_{l_{fMRI}=1}^{L_{fMRI}} U_{l_{fMRI}}(\boldsymbol{k}) V_{l_{fMRI}}(T) \tag{4.8}$$

where $\left\{V_{l_{fMRI}}(T)\right\}_{l_{fMRI}=1}^{L_{fMRI}}$ is the set of temporal basis functions for fMRI signals, $\left\{U_{l_{fMRI}}(\boldsymbol{k})\right\}_{l_{fMRI}=1}^{L_{fMRI}}$ are the corresponding coefficients, and L_{fMRI} is the rank of the model, which indicates the order of separability. In functional imaging, the PS model can be justified because the BOLD signals come from finite number of functional networks and each of them has a distinct signal variation structure, which means the number of basis functions to represent the signals should be finite.

To reconstruct the fMRI images from the temporally under-sampled data, first, we need to overcome the Nyquist ghost caused by the eddy current-induced inconsistency between readouts of different polarity. This correction is done using the information from a five-second calibration scan that is acquired during the preparation period of the sequence. The k-space shift and phase difference between positive and negative readout can be estimated from the acquired calibration scan and then applied to correct the inconsistency in $d_1(\boldsymbol{k}, T)$. This correction eliminates the Nyquist ghost in the following reconstruction.

Then, we can solve the reconstruction problem based on the subspace model. This reconstruction is quite similar to the reconstruction in MRSI signal since both the fMRI signals and MRSI signals are temporally under-sampled. But the differences are that MRSI

is sparsely sample in t while fMRI is sparsely sampled in T. Also the temporal basis function of fMRI can be estimated from the data itself, but this cannot be done for MRSI so it depends on the physical prior and training data. Similarly, the reconstruction can also be divided into two steps: a) determination of the temporal basis and b) estimation of the corresponding spatial coefficients. Under the acquisition scheme shown in Fig. 3.6, there are 10 phase encodings in kz (encoded in 2 TRs) that are commonly acquired in both 8TR and 2TR frames. It means, in these k-space locations, the fMRI signals are temporally fully sampled. Therefore, the temporal basis functions can be estimated from the $d_1(\boldsymbol{k}, T)$ in these k-space locations. More specifically, using the $d_1(\boldsymbol{k}, T)$ in these k-space locations can form a $\mathrm{N_k} \times \mathrm{N_T}$ Casorati matrix. Then, SVD is applied on this Casorati matrix and its leading L_{fMRI} principle right singular vectors can be chosen as $\left\{V_{l_{fMRI}}(T)\right\}_{l_{fMRI}=1}^{L_{fMRI}}$ which can actually be a set of temporal basis functions. After the temporal basis functions are determined, the corresponding coefficients $\left\{U_{l_{fMRI}}(\boldsymbol{k})\right\}_{l_{fMRI}=1}^{L_{fMRI}}$ can be estimated from the sparsely sampled $\mathrm{d_1}(\mathbf{k}, \mathrm{T})$ by solving a constrained optimization problem:

$$\widehat{\boldsymbol{U}}_{fMRI} = \arg\min_{\boldsymbol{U}_{fMRI}} ||\boldsymbol{d}_1 - \Omega_1 \mathcal{F} \boldsymbol{U}_{fMRI} \boldsymbol{V}_{fMRI}||_2^2 + \lambda ||\boldsymbol{W} \boldsymbol{U}_{fMRI}||_2^2 \tag{4.9}$$

where $\mathbf{U}_{\mathrm{fMRI}}$, $\mathbf{V}_{\mathrm{fMRI}}$ and $\mathbf{d_1}$ denote the matrix representation of spatial coefficients to be estimated, obtained temporal basis functions from the data and the measured data in $d_1(\boldsymbol{k}, T)$, respectively. Ω_1 is the $(\boldsymbol{k}, T)$ space sampling operator as shown in Fig. 3.6. $\mathbf{W}$ is a diagonal weighting matrix to impose different penalty weight on $\mathbf{U}_{\mathrm{fMRI}}$. After determining the coefficients, the reconstructed dataset $\hat{d}_1(\boldsymbol{k}, T)$ can be obtained by combining the spatial coefficients and temporal bases functions.

$$\hat{d}_1(\boldsymbol{k}, T) = \sum_{l_{fMRI}=1}^{L_{fMRI}} \widehat{U}_{l_{fMRI}}(\boldsymbol{k}) V_{l_{fMRI}}(T) \tag{4.10}$$

In summary, the reconstruction of fMRI images is also based on the subspace modeling and the basis function can estimated from the data itself. The reconstruction method can also be extended to lots of dynamic imaging applications.

4.4 Optimization using Complementary Information between fMRI and MRSI

As mentioned in data acquisition, one of the advantages of simultaneous acquisition of both fMRI and MRSI is that we can utilize the complementary information between fMRI and MRSI to enable high quality reconstruction and removal of artifacts.

On the one hand, using the complementary information from MRSI, we are able to solve several data processing problems for fMRI data, which include: 1) correction of chemical shift effect of lipid signals, 2) correction of geometric distortion caused by field inhomogeneity and 3) signal drop-out caused by large susceptibility effect.

The chemical shift of lipid signals mainly comes from the low encoding bandwidth in the phase encoding direction (ky and kz). In traditional fMRI protocols, the lipid signal is suppressed using spectral selective pulses [47]. Using these suppression pulses can overcome the chemical shift effect, but also increases the RF power and prolongs the TR to increase scanning time. Under the proposed data acquisition scheme, it can be addressed by signal processing using complementary information from MRSI. In general, we can obtain the lipid distribution from the MRSI dataset $d_2(\boldsymbol{k}, t)$, which provides the spatiotemporal function of the lipid signals. More specifically, we can first identify the lipid region of the subcutaneous layer with a tissue segmentation and then obtain the spatiospectral functions of pure lipid signals, denoted as $\rho_f(\boldsymbol{x}, t)$. Then, from $\rho_f(\boldsymbol{x}, t)$ and the known encoding timing and k-space location of the EVI sampling trajectory, the lipid signal distribution in fMRI dataset $d_1(\boldsymbol{k}, T)$ can be fully calculated. Subtracting the calculated fat signal from $d_1(\boldsymbol{k}, T)$ can remove the shifted fat signals, which may overlap with the brain tissue.

The geometric distortion and signal loss near the sinus region are mostly due to large field variation caused by field inhomogeneity or bad susceptibility effect. To solve this problem, the key issue is to get the accurate, high resolution field distribution. As described in section 4.2, we can derive a high-resolution field map from the unsuppressed water signal through an HSVD fitting. This field map can be used in correcting the field effect not only in MRSI

but also in fMRI. More specifically, the accumulated phase induced by the field can be eliminated from the simulated spatiotemporal functions of $d_1(\boldsymbol{k}, t, T)$ from $d_2(\boldsymbol{k}, t)$ for each frame. This removal of phase caused by field effect can fix both the geometric distortion and large signal-loss near the bad susceptibility region. In typical fMRI experiments, to overcome the geometric distortion problem, additional scans are required to measure and map the field map or the point spread functions in the same encoding setting [52]. And some additional scans, like z-shim [53], are also used for compensating the signal drop-out. These methods all require additional scans but none is needed in our proposed method, which can save acquisition time and also provide a unique processing routine to tackle these problems.

On the other hand, the complementary information from fMRI can also help improve the image quality of MRSI. The first one is the correction of field drift, as described in section 4.2. Another advantage of this simultaneous acquisition is that the fMRI data $d_1(\boldsymbol{k}, T)$ can play the role of motion navigators for the MRSI data. The fMRI data are collected in high temporal resolution (3 seconds), and in true 3D volume, so the bulk head motion during the scan can be captured very well by the fMRI signals. Determining the head motion parameters from the reconstructed fMRI images, we are able to correct motion effects in the MRSI data and thus remove the motion artifacts. This capability to correct the motion effect will greatly increase the robustness of MRSI acquisition and reconstruction.

5. Results and Discussion

In this chapter, the representative results are presented to demonstrate the unprecedented imaging capability to enable simultaneous acquisition of high-resolution fMRI and MRSI signals and the high-quality reconstruction of functional networks and metabolite spatiospectral functions.

5.1 ^{1}H-MRSI Results

Figure 5.1 shows a set of representative MRSI results from the 6-minute simultaneous fMRI-MRSI scan. As described in the section 3.4, the ^{1}H-MRSI experiment uses the sequence with: Flip angle = 27°, TR = 160 ms, TE = 1.6 ms, readout bandwidth = 167 kHz, FOV = 230 × 230 × 72 mm^3 with two outer volume suppression (OVS) bands. The resulting nominal spatial resolution is 1.9 × 2.3 × 3.0 mm. Both the reconstructed high-resolution metabolic maps and spatially resolved spectra are displayed. The metabolite maps obtained include N-acetylaspartate (NAA), creatine (Cre), choline (Cho) and myo-inositol (mI). It can be observed that high resolution, high quality metabolite maps, as well as the high SNR spectra, can be obtained from a 6-minute scan. The representative spectra from three different spatial positions also show the spatial variation, and we can easily distinguish the several most dominant metabolite peaks from the spectra.

Figure 5.2 presents a set of results using the complementary information from fMRI to improve the quality and robustness of MRSI. The frequency drift curve is estimated from the field drift navigator embedded in the fMRI acquisition. The motion curves include rotation, and translation parameters are estimated from the reconstructed fMRI images using image registration method. Then both the field drift and motion information are applied in MRSI processing to correct the effects. We can see that the motion curves capture the subject motion in high temporal resolution (around 3 seconds). Without motion correction, there exist obvious artifacts on the metabolite maps. These artifacts are largely reduced after motion correction and it results in much more reasonable metabolite maps (the NAA and Cre maps are shown). In a clinical setting, the patient motion is usually

inevitable. The capability to correct the motion artifacts in MRSI data can significantly improve the robustness of MRSI reconstruction quality.

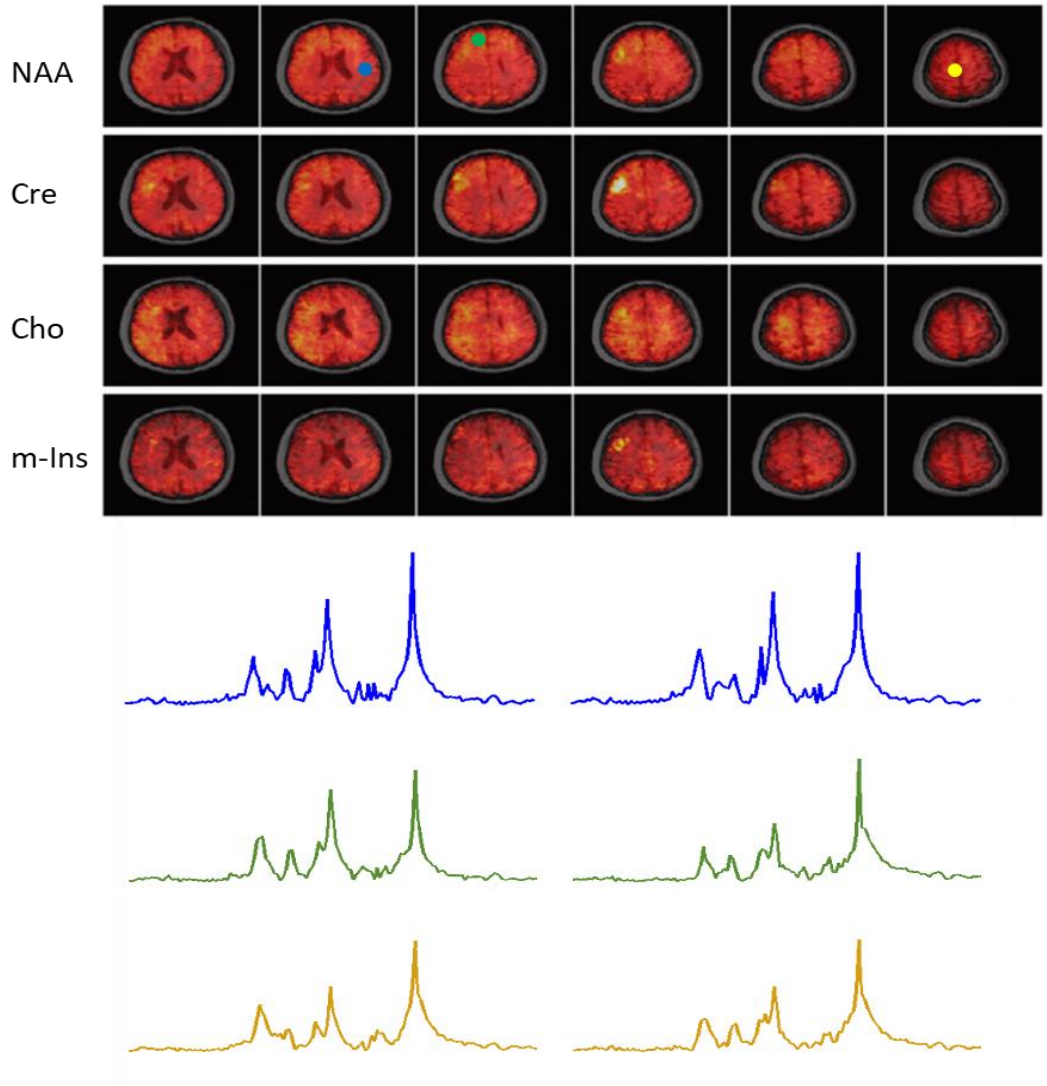

Figure 5.1: The reconstructed high-resolution metabolic maps and spatially resolved spectra in selected spatial location. The metabolite maps obtained include but are not limited to N-acetylaspartate (NAA), creatine (Cre), choline (Cho) and myo-inositol (mI). The high-quality spatiospectral functions of metabolites are reconstructed from a 6-minute simultaneous fMRI-MRSI scan. Each metabolite map is normalized individually and displayed as the colormap overlaid on anatomical images.

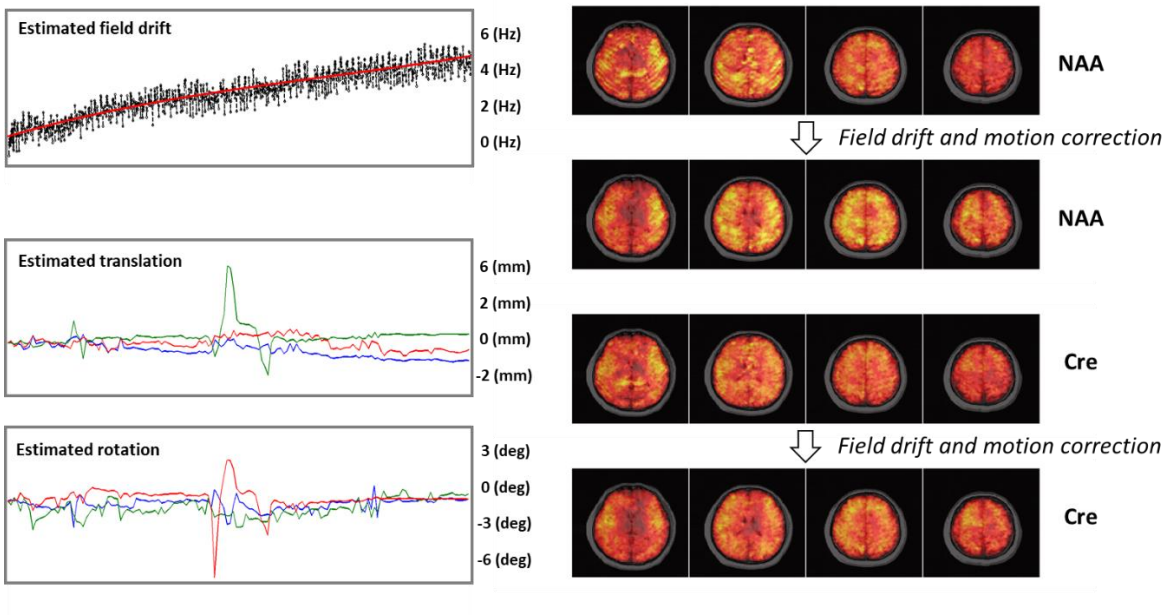

Figure 5.2: The effect of field drift correction and motion correction. The left column shows the estimated frequency drift curve from the field drift navigator, and the 6-paramter rigid body motion curves estimated from the fMRI images. The right column shows the reconstructed metabolite maps including NAA and Cre before and after the motion correction. It is obvious that the motion artifacts are significantly reduced after the motion correction using the motion information from fMRI images.

5.2 fMRI Results

The functional imaging results for both resting-state and task-based experiments are shown in Figs. 5.3-5.5. These scans are also the simultaneous fMRI-MRSI scans which took 6 minutes. The resting-state networks are displayed in Fig. 5.3. These functional networks are extracted from the fMRI images using ICA based methods [39], [40] and the network components are manually sorted out. The spatial resolution of these functional network maps is $3.0 \times 3.0 \times 1.8$ mm^3 and temporal resolution of the image series is 3 seconds. The displayed functional networks include: default mode network (DWN), visual cortex network (VCN), somato-motor network (SMN) and auditory cortex network (ACN). The network structures are consistent with previous studies using typical multi-slice EPI sequence.

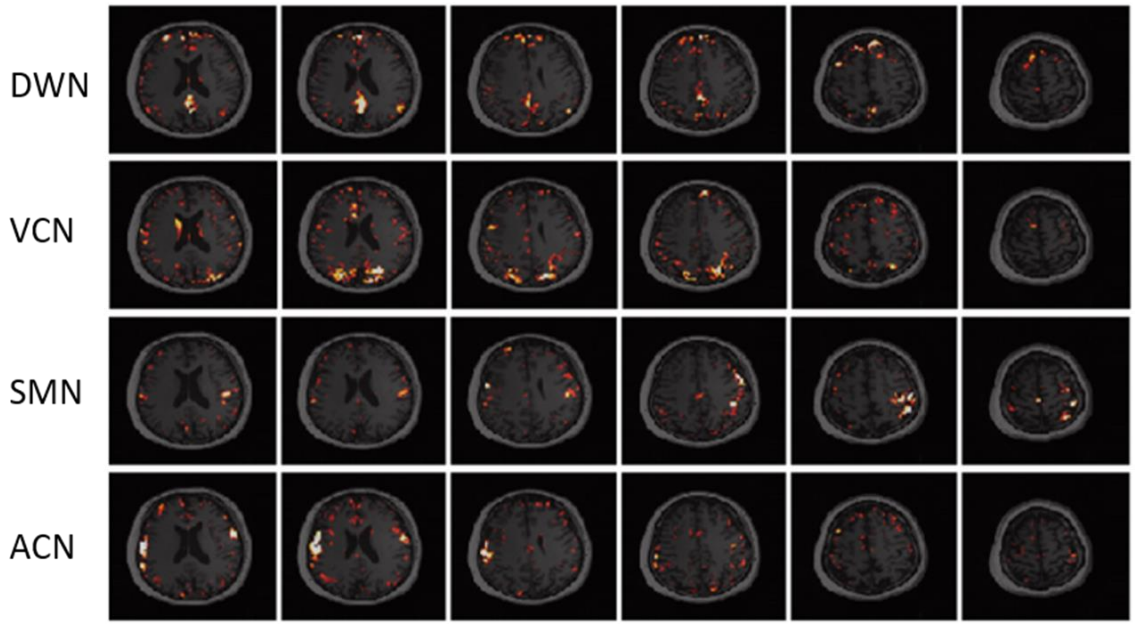

Figure 5.3: IC maps representing resting-state functional networks from the simultaneous fMRI and MRSI scan. IC maps are displayed with threshold $|z| > 2$. From top to bottom: default mode network (DWN), visual cortex network (VCN), somato-motor network (SMN), auditory cortex network (ACN). The spatial structure of the functional networks is consistent with the previously reported studies [54], [55].

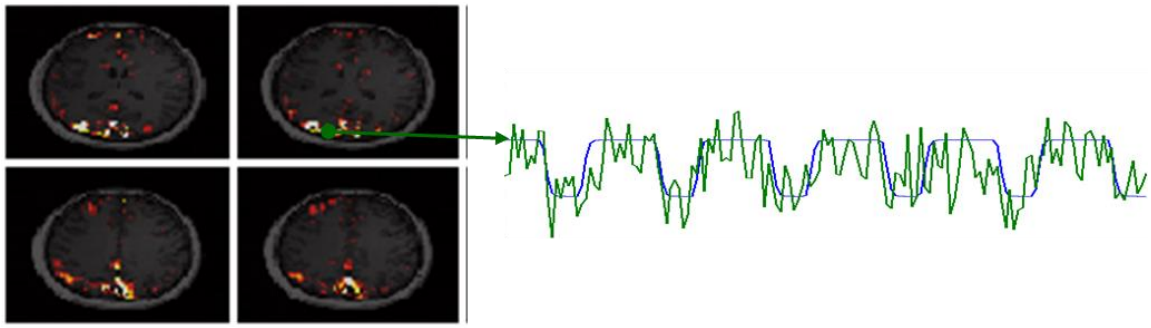

Figure 5.4: The visual cortex network and its corresponding time course obtained from a simultaneous fMRI-MRSI scan. The subject was visually stimulated during the task frames and at rest during the resting frames. The obtained time course shows a high correlation with the reference function generated from the designed event blocks.

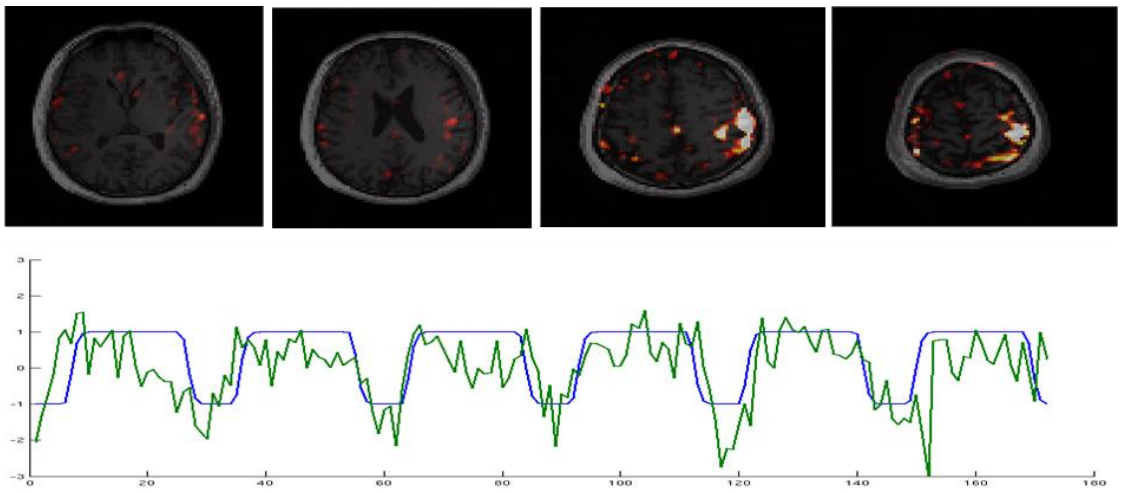

Figure 5.5: The motor cortex network and its corresponding time course obtained from a simultaneous fMRI-MRSI scan. The subject was instructed to perform finger tapping task using right hand only during the scan. The obtained time course shows a high correlation with the reference function generated from the designed event blocks.

The results of task-based experiments are shown in Fig. 5.4 and Fig. 5.5. Figure 5.4 shows the visual cortex network and its corresponding time course. In this visual stimulation experiment, the subject was stimulated by visual figures during the stimulation block and kept eyes open and fixated on a cross during the resting blocks. The obtained time course shows a high correlation with the reference function generated from the designed event blocks, which demonstrates the sensitivity of our method to capture the functional activities due to visual stimulation. Figure 5.5 shows another motor task experiment. The obtained time course and the motor cortex network are within the expectation and match the literature [54], [55].

Figure 5.6 presents the processing results using the complementary information from MRSI signals. As mentioned in section 4.3, using MRSI information helps to remove the chemical shift of lipid signals and correct the geometric distortion and susceptibility-induced signal loss due to large field variations. These corrections were done with no additional cost instead of the typical routines involving suppression pulses or additional calibration scans. The functional networks are usually extracted from the artifact-corrected data.

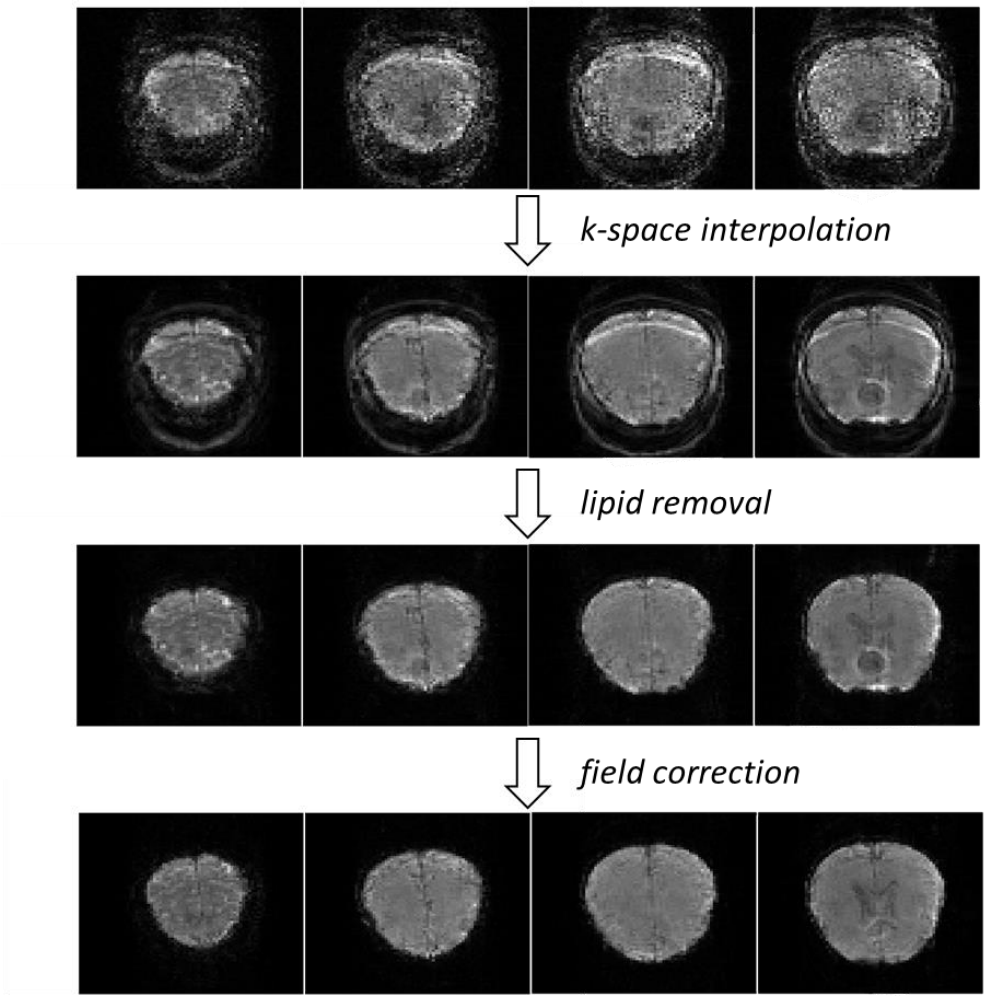

Figure 5.6: The results of processing using complementary information from MRSI, which contains the lipid removal and correction of geometric distortion and signal drop-off caused by the field variation.

In summary, this chapter presents some representative MRSI and fMRI results to demonstrate the imaging capability of the proposed method and also show the advantages of using the complementary information between MRSI and fMRI to improve the quality of each.

6. Conclusions

This thesis has proposed a new method to enable simultaneous fMRI and MRSI of the brain. In contrast to the current acquisition scheme for fMRI and MRSI, which acquires images in separate scans, our proposed method integrates SPICE-based MRSI with EVI-based fMRI in an interleaved fashion. The acquisition also incorporates ramp sampling, sparse sampling, ultra-short TE and short TR strategy to enable high spatiotemporal resolution for both fMRI and MRSI. The signal processing and image reconstruction are mostly based on the subspace and partial separability modeling. The complementary information between fMRI and MRSI is also utilized to enable high quality reconstruction and improvement of robustness. The preliminary experimental results have demonstrated an unprecedented capability of our proposed method in simultaneous functional and metabolic imaging of the brain at high resolution. The technique, when fully developed, may provide a powerful tool to study brain function and metabolism under both normal and diseased conditions.

References

[1] S. Ogawa, T. M. Lee, A. R. Kay, and D. W. Tank, “Brain magnetic resonance imaging with contrast dependent on blood oxygenation.,” *Proc. Natl. Acad. Sci.*, vol. 87, no. 24, pp. 9868–9872, 1990.

[2] J. W. Belliveau *et al.*, “Functional mapping of the human visual cortex by magnetic resonance imaging,” *Science.*, vol. 254, no. 5032, pp. 716–719, 1991.

[3] P. A. Bandettini, E. C. Wong, R. S. Hinks, R. S. Tikofsky, and J. S. Hyde, “Time course EPI of human brain function during task activation,” *Magn. Reson. Med.*, vol. 25, no. 2, pp. 390–397, 1992.

[4] K. K. Kwong *et al.*, “Dynamic magnetic resonance imaging of human brain activity during primary sensory stimulation,” *Proc. Natl. Acad. Sci.*, vol. 89, no. 12, pp. 5675–5679, 1992.

[5] B. Biswal, F. Zerrin Yetkin, V. M. Haughton, and J. S. Hyde, “Functional connectivity in the motor cortex of resting human brain using echo-planar MRI,” *Magn. Reson. Med.*, vol. 34, no. 4, pp. 537–541, 1995.

[6] P. A. Bandettini, E. C. Wong, A. Jesmanowicz, R. S. Hinks, and J. S. Hyde, “Spin-echo and gradient-echo EPI of human brain activation using bold contrast: A comparative study at 1.5 T,” *NMR Biomed.*, vol. 7, no. 1–2, pp. 12–20, 1994.

[7] P. C. Lauterbur, D. M. Kramer, W. V. House, and C. N. Chen, “Zeugmatographic high resolution nuclear magnetic resonance spectroscopy. images of chemical inhomogeneity within macroscopic objects,” *Journal of the American Chemical Society*, vol. 97, no. 23. pp. 6866–6868, 1975.

[8] T. R. Brown, B. M. Kincaid, and K. Ugurbil, “NMR chemical shift imaging in three dimensions,” *Proc. Natl. Acad. Sci.*, vol. 79, no. 11, pp. 3523–3526, 1982.

[9] A. A. Maudsley, S. K. Hilal, W. H. Perman, and H. E. Simon, “Spatially resolved high resolution spectroscopy by ‘four-dimensional’ NMR,” *J. Magn. Reson.*, vol. 51, no. 1, pp. 147–152, 1983.

[10] P. Mansfield, “Spatial mapping of the chemical shift in NMR,” *Magn. Reson. Med.*, vol. 1, no. 3, pp. 370–386, 1984.

[11] S. Posse, G. Tedeschi, R. Risinger, R. Ogg, and D. Le Bihan, “High speed 1H spectroscopic imaging in human brain by echo planar spatial-spectral encoding,” *Magn. Reson. Med.*, vol. 33, no. 1, pp. 34–40, 1995.

[12] A. A. Maudsley *et al.*, “Mapping of brain metabolite distributions by volumetric proton MR spectroscopic imaging (MRSI),” *Magn. Reson. Med.*, vol. 61, no. 3, pp. 548–559, 2009.

[13] S. Posse, R. Otazo, S. R. Dager, and J. Alger, "MR spectroscopic imaging: Principles and recent advances," *Journal of Magnetic Resonance Imaging*, vol. 37, no. 6. pp. 1301–1325, 2013.

[14] J. Prichard *et al.*, "Lactate rise detected by 1H NMR in human visual cortex during physiologic stimulation.," *Proc. Natl. Acad. Sci.*, vol. 88, no. 13, pp. 5829–5831, 1991.

[15] J. Frahm, G. Krüger, K. D. Merboldt, and A. Kleinschmidt, "Dynamic uncoupling and recoupling of perfusion and oxidative metabolism during focal brain activation in man," *Magn. Reson. Med.*, vol. 35, no. 2, pp. 143–148, 1996.

[16] W. Chen, E. J. Novotny, X.-H. Zhu, D. L. Rothman, and R. G. Shulman, "Localized 1H NMR measurement of glucose consumption in the human brain during visual stimulation," *Proc. Natl. Acad. Sci. U. S. A.*, vol. 90, no. 21, pp. 9896–900, 1993.

[17] P. G. Mullins, L. M. Rowland, R. E. Jung, and W. L. Sibbitt, "A novel technique to study the brain's response to pain: Proton magnetic resonance spectroscopy," *Neuroimage*, vol. 26, no. 2, pp. 642–646, 2005.

[18] D. Sappey-Marinier, G. Calabrese, G. Fein, J. W. Hugg, C. Biggins, and M. W. Weiner, "Effect of photic stimulation on human visual cortex lactate and phosphates using 1H and 31P magnetic resonance spectroscopy," *J. Cereb. Blood Flow Metab.*, vol. 12, no. 4, pp. 584–592, 1992.

[19] S. Mangia *et al.*, "Sensitivity of single-voxel 1H-MRS in investigating the metabolism of the activated human visual cortex at 7 T," *Magn. Reson. Imaging*, vol. 24, no. 4, pp. 343–348, 2006.

[20] S. Mangia, I. Tkáč, R. Gruetter, P. F. Van De Moortele, B. Maraviglia, and K. Uğurbil, "Sustained neuronal activation raises oxidative metabolism to a new steady-state level: Evidence from 1H NMR spectroscopy in the human visual cortex," *J. Cereb. Blood Flow Metab.*, vol. 27, no. 5, pp. 1055–1063, 2007.

[21] J. M. N. Duarte, H. Lei, V. Mlynárik, and R. Gruetter, "The neurochemical profile quantified by in vivo 1H NMR spectroscopy," *NeuroImage*, vol. 61, no. 2. pp. 342–362, 2012.

[22] Y. Lin, M. C. Stephenson, L. Xin, A. Napolitano, and P. G. Morris, "Investigating the metabolic changes due to visual stimulation using functional proton magnetic resonance spectroscopy at 7 T," *J. Cereb. Blood Flow Metab.*, vol. 32, no. 8, pp. 1484–1495, 2012.

[23] B. Schaller, R. Mekle, L. Xin, N. Kunz, and R. Gruetter, "Net increase of lactate and glutamate concentration in activated human visual cortex detected with magnetic resonance spectroscopy at 7 tesla," *J. Neurosci. Res.*, vol. 91, no. 8, pp. 1076–1083, 2013.

[24] M. A. Griswold *et al.*, "Generalized Autocalibrating Partially Parallel Acquisitions (GRAPPA)," *Magn. Reson. Med.*, vol. 47, no. 6, pp. 1202–1210, 2002.

[25] K. P. Pruessmann, M. Weiger, M. B. Scheidegger, and P. Boesiger, "SENSE: Sensitivity encoding for fast MRI," *Magn. Reson. Med.*, vol. 42, no. 5, pp. 952–962, 1999.

[26] D. J. Larkman, J. V. Hajnal, A. H. Herlihy, G. A. Coutts, I. R. Young, and G. Ehnholm, "Use of multicoil arrays for separation of signal from multiple slices simultaneously excited," *J. Magn. Reson. Imaging*, vol. 13, no. 2, pp. 313–317, 2001.

[27] E. Adalsteinsson, P. Irarrazabal, S. Topp, C. Meyer, A. Macovski, and D. M. Spielman, "Volumetric spectroscopic imaging with spiral-based k-space trajectories," *Magn. Reson. Med.*, vol. 39, no. 6, pp. 889–898, 1998.

[28] F. Lam and Z. P. Liang, "A subspace approach to high-resolution spectroscopic imaging," *Magn. Reson. Med.*, vol. 71, no. 4, pp. 1349–1357, 2014.

[29] Z. P. Liang, "Spatiotemporal imaging with partially separable functions," in *Proc. of 2007 Joint Meet. of the 6th Int. Symp. on Noninvasive Functional Source Imaging of the Brain and Heart and the Int. Conf. on Functional Biomedical Imaging, NFSI and ICFBI 2007*, 2007, pp. 181–182.

[30] X. Peng, F. Lam, Y. Li, B. Clifford, and Z. P. Liang, "Simultaneous QSM and metabolic imaging of the brain using SPICE," *Magn. Reson. Med.*, vol. 79, no. 1, pp. 13–21, 2018.

[31] X. Hu, D. N. Levin, P. C. Lauterbur, and T. Spraggins, "SLIM: Spectral localization by imaging," *Magn. Reson. Med.*, vol. 8, no. 3, pp. 314–322, 1988.

[32] M. Lustig, D. Donoho, and J. M. Pauly, "Sparse MRI: The application of compressed sensing for rapid MR imaging," *Magn. Reson. Med.*, vol. 58, no. 6, pp. 1182–1195, 2007.

[33] H. M. Nguyen, X. Peng, M. N. Do, and Z. P. Liang, "Denoising MR spectroscopic imaging data with low-rank approximations," *IEEE Trans. Biomed. Eng.*, vol. 60, no. 1, pp. 78–89, 2013.

[34] J. Kasten, A. Klauser, F. Lazeyras, and D. Van De Ville, "Magnetic resonance spectroscopic imaging at superresolution: Overview and perspectives," *Journal of Magnetic Resonance*, vol. 263. pp. 193–208, 2016.

[35] P. C. M. van Zijl, C. T. W. Moonen, J. R. Alger, J. S. Cohen, and S. A. Chesnick, "High field localized proton spectroscopy in small volumes: greatly improved localization and shimming using shielded strong gradients," *Magn. Reson. Med.*, vol. 10, no. 2, pp. 256–265, 1989.

[36] C. T. W. Moonen *et al.*, "Comparison of single-shot localization methods (steam and press) for In vivo proton NMR spectroscopy," *NMR Biomed.*, vol. 2, no. 5–6, pp. 201–208, 1989.

[37] J. Slotboom, A. F. Mehlkopf, and W. M. M. J. Bovée, "A single-shot localization pulse sequence suited for coils with inhomogeneous RF fields using adiabatic slice-selective RF pulses," *J. Magn. Reson.*, vol. 95, no. 2, pp. 396–404, 1991.

[38] T. W. J. Scheenen, D. W. J. Klomp, J. P. Wijnen, and A. Heerschap, "Short echo time 1H-MRSI of the human brain at 3T with minimal chemical shift displacement errors using adiabatic refocusing pulses," *Magn. Reson. Med.*, vol. 59, no. 1, pp. 1–6, 2008.

[39] M. J. McKeown *et al.*, "Analysis of fMRI data by blind separation into independent spatial components," *Hum. Brain Mapp.*, vol. 6, no. 3, pp. 160–188, 1998.

[40] C. F. Beckmann and S. M. Smith, "Probabilistic independent component analysis for functional magnetic resonance imaging," *IEEE Trans. Med. Imaging*, vol. 23, no. 2, pp. 137–152, 2004.

[41] A. Hyvärinen and E. Oja, "A fast fixed-point algorithm for independent component analysis," *Neural Comput.*, vol. 9, no. 7, pp. 1483–1492, 1997.

[42] B. Schaller, L. Xin, K. O'Brien, A. W. Magill, and R. Gruetter, "Are glutamate and lactate increases ubiquitous to physiological activation? A 1H functional MR spectroscopy study during motor activation in human brain at 7 Tesla," *Neuroimage*, vol. 93, no. P1, pp. 138–145, 2014.

[43] Z. Huang *et al.*, "Increase in glutamate/glutamine concentration in the medial prefrontal cortex during mental imagery: A combined functional mrs and fMRI study," *Hum. Brain Mapp.*, vol. 36, no. 8, pp. 3204–3212, 2015.

[44] P. Bednařík *et al.*, "Neurochemical and BOLD responses during neuronal activation measured in the human visual cortex at 7 Tesla," *J. Cereb. Blood Flow Metab.*, vol. 35, pp. 601–610, 2015.

[45] L. A. Jelen, S. King, P. G. Mullins, and J. M. Stone, "Beyond static measures: A review of functional magnetic resonance spectroscopy and its potential to investigate dynamic glutamatergic abnormalities in schizophrenia," *Journal of Psychopharmacology*, vol. 32, no. 5. pp. 497–508, 2018.

[46] F. Lam, C. Ma, B. Clifford, C. L. Johnson, and Z. P. Liang, "High-resolution1H-MRSI of the brain using SPICE: Data acquisition and image reconstruction," *Magn. Reson. Med.*, vol. 76, no. 4, pp. 1059–1070, 2016.

[47] A. Haase, J. Frahm, W. Hanicke, and D. Matthaei, "1H NMR chemical shift selective (CHESS) imaging," *Plasma Sources Sci. Technol.*, vol. 30, no. 4, pp. 341–344, 1985.

[48] C. Ma, F. Lam, C. L. Johnson, and Z. P. Liang, "Removal of nuisance signals from limited and sparse1H MRSI data using a union-of-subspaces model," *Magn. Reson. Med.*, vol. 75, no. 2, pp. 488–497, 2016.

[49] A. Papoulis, "Generalized sampling expansion," *IEEE Trans. Circuits Syst.*, vol. 24, no. 11, pp. 652–654, 1977.

[50] L. Vanhamme, A. Van Den Boogaart, and S. Van Huffel, "Improved method for accurate and efficient quantification of MRS data with use of prior knowledge," *J. Magn. Reson.*, vol. 129, no. 1, pp. 35–43, 1997.

[51] Y. Li, F. Lam, R. Guo, B. Clifford, X. Peng, and Z. Liang, "Removal of water sidebands from 1H-MRSI data acquired without water suppression," in *In Proceedings of the International Symposium on Magnetic Resonance in Medicine*, 2017.

[52] P. Jezzard, "Correction of geometric distortion in fMRI data," *NeuroImage*, vol. 62, no. 2. pp. 648–651, 2012.

[53] G. H. Glover, "3D Z-shim method for reduction of susceptibility effects in BOLD fMRI," *Magn. Reson. Med.*, vol. 42, no. 2, pp. 290–299, 1999.

[54] M. H. Lee, C. D. Smyser, and J. S. Shimony, "Resting-state fMRI: A review of methods and clinical applications," *Am. J. Neuroradiol.*, vol. 34, no. 10, pp. 1866–1872, 2013.

[55] G. Doucet *et al.*, "Brain activity at rest: a multiscale hierarchical functional organization," *J. Neurophysiol.*, vol. 105, no. 6, pp. 2753–2763, 2011.